Indian Journal of Biochemistry & Biophysics
Vol. 63, August 2026, pp. 904-922
DOI: 10.56042/ijbb.v63i8.23452

Influence of variable viscosity and nonlinear radiation on heat and mass transfer in rotating ternary nanofluid flow over a stretching sheet

Gayathri Pappur[1], and Chandrakala Panguluri[2]*

[1]Department of Mathematics, Government Degree College, Puttur-517 583, Andhra Pradesh, India

[2]Department of Mathematics, School of Engineering, Anurag University, Hyderabad-500 088, Telangana, India

Received 04 September 2025; *revised 12 April 2026*

The accelerating thermal demands of contemporary energy, electronic and biomedical systems have rendered conventional working fluids inadequate for high-flux heat dissipation. Mono- and binary-hybrid nanofluids partially address this deficit, yet the synergistic potential of three dissimilar nanoparticles dispersed in a single base fluid remains insufficiently characterised, particularly under the simultaneous action of rotation, temperature-dependent viscosity and nonlinear thermal radiation. The present investigation is motivated by this gap and seeks to quantify how a water-based ternary nanofluid composed of copper, alumina and silver ($Cu–Al_2O_3–Ag/H_2O$) responds, in a rotating frame, to the coupled influence of partial velocity slip, Arrhenius activation energy, Newtonian cooling and nonlinear thermal radiation. The governing partial differential equations are reduced to a set of nonlinear, coupled ordinary differential equations through suitable similarity transformations and are integrated numerically by employing a fifth-order Runge–Kutta–Fehlberg algorithm coupled with the shooting technique. Rigorous validation against previously reported limiting-case solutions establishes the fidelity of the present scheme. The hydrodynamic, thermal and concentration fields are interrogated systematically with respect to all pertinent physical parameters, and the engineering quantities of interest; skin friction coefficient, local nusselt number and local sherwood number are tabulated. The numerical experiments reveal that the axial velocity is attenuated by augmentation of the slip parameter, the viscosity parameter and the nonlinear radiation parameter, whereas it is amplified by the Newtonian cooling parameter. The thermal field is enhanced by viscous dissipation, Brownian diffusion and thermophoresis, and the ternary suspension consistently outperforms its binary-hybrid counterpart in terms of heat transport efficiency. The findings furnish quantitative guidance for the design of advanced thermal-management devices that exploit multi-component nanofluids.

Keywords: Activation energy, Arrhenius kinetics, Brownian motion, Hall current, Newtonian cooling, Partial slip, Thermophoresis

Since stretching surfaces are important in many industrial and engineering applications, fluid mechanics has focused on them. Polymer extrusion, metal shaping, and cooling of electrical and biological equipment use such surfaces. One of the first analytical studies on viscous fluid flow over two-dimensional stretching sheets. Crane[1] added flows over extending cylinders with linearly varying velocity. Wang[2] studied heat transmission and fluid motion outside stretching cylinders. Later, the effects of magnetic fields on spinning, stretching cylinders were quantitatively explored using bvp4c methods[3,4]. Choi[5] created nanofluids to improve heat conductivity by adding nanoparticles like copper (Cu), silver (Ag), and aluminum oxide (Al_2O_3) to base fluids. Later, Buongiorno[6] discovered that Brownian motion and thermophoresis control nanoparticle mobility in these fluids. Nanofluids have long been utilized in electronic cooling, medical equipment, and heat exchangers. Based on this, researchers created hybrid nanofluids with two nanoparticle kinds to boost thermal performance. Researchers Hayat and Nadeem[7], and Waqas *et al*.[8] studied the performance of $Ag-TiO_2-Al_2O_3$/water hybrid nanofluids in rotating systems with torsional motion. These hybrid combinations have enhanced heat conductivity and adaptability in power plants, diagnostic medical equipment, and refrigerated cooling systems, making them promising for advanced heat transfer applications. Uma Devi and Anjali Devi[9] studied $Al_2O_3–Cu$/water hybrid nanofluids on linearly extending surfaces. Acharya *et al*.[10] studied magnetic field hybrid nanofluid flow with surface slip. Al-Mdallal and Usman[11] examined hybrid nanofluids on permeable surfaces. Hybrid nanofluid flows in

*Correspondence:
E-mail:chandrakalapanguluri@gmail.com

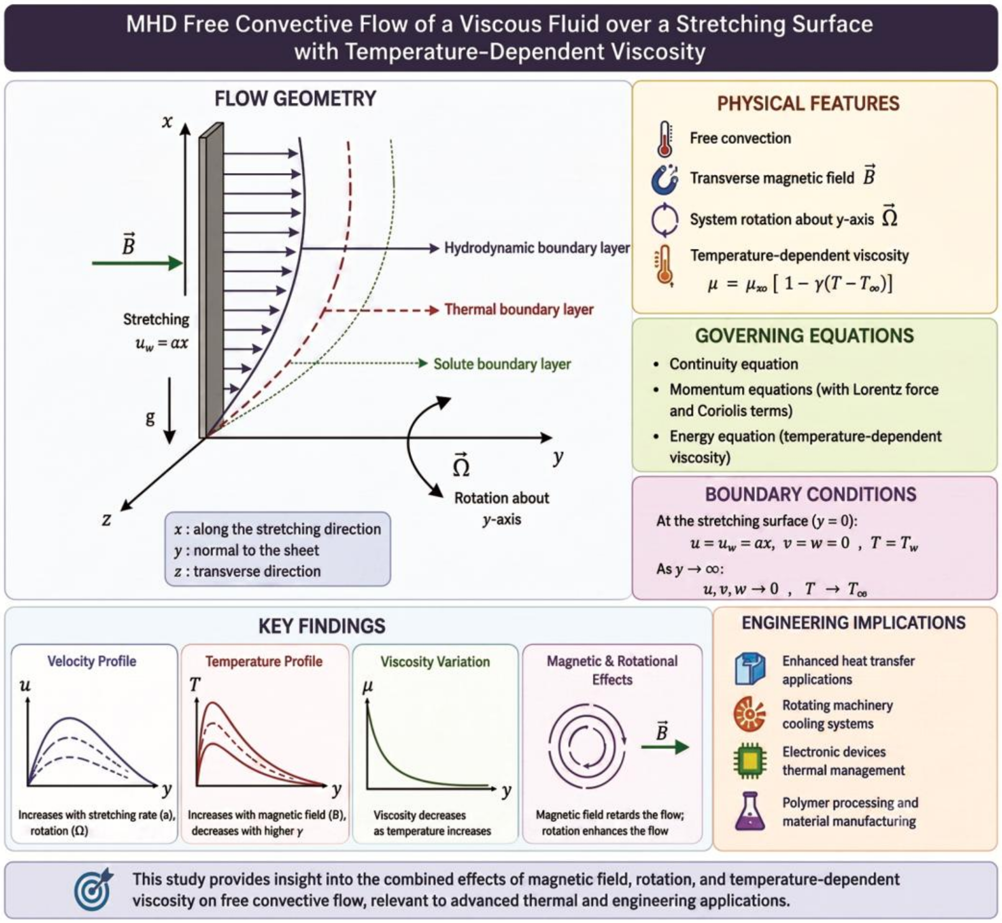

Graphical abstract

magnetohydrodynamic (MHD) porous media have been advanced by Emad *et al*.[12] and Khan *et al*.[13]. Mousavi *et al*.[14] and Sahoo and Kumar[15] examined how temperature and nanoparticle volume fraction affect the thermal behavior of CuO-MgO-TiO_2 and Al_2O_3-CuO-TiO_2/water nanofluids Chandrakala and Srinivasa Rao[16] examined how dissipation and chemical reaction affect ternary nanofluid flow across a stretching sheet in porous media. The partial slip boundary condition applies to nanofluid flows with limited fluid-surface adhesion. Ullah *et al*.[17] studied velocity slip and Newtonian heating in Casson fluid flow across a nonlinear stretching surface. Hayat *et al*.[18], Jusoh *et al*.[19], and others have researched slip in three-dimensional flows over permeable boundaries.

A fundamental aspect in reactive nanofluid flows is activation energy, the minimal energy needed to start chemical reactions. Krishna *et al*.[20] examined how Hall currents affect MHD convective behavior, whereas Roy and Pal[21] examined Casson nanofluid flows in MHD with nonlinear radiation and Ohmic heating. Activation energy associated with chemical reactions can significantly influence the convective heat and mass transfer characteristics of nanofluids, particularly over non-uniform or stretching surfaces. In this context, Yesodha *et al*.[22] analyzed nanofluid flow with activation energy and heat generation/absorption effects over a stretching surface under convective boundary conditions and showed that higher activation energy enhances the species diffusion rate, thereby modifying the thermal boundary layer and convective heat-transfer performance. Similarly, Sardar *et al*.[23] investigated the impact of activation energy on Carreau nanofluid flow over a nonlinear stretching surface and reported that increasing activation energy strengthens the mass-transfer rate while also altering the momentum and thermal distributions, highlighting the coupling between chemical kinetics and convective transport. These findings collectively indicate that activation energy can act as a controlling parameter in convective nanofluid heat-transfer systems, especially when the surface geometry or stretch rate is non-uniform.

In energy, medicinal, and aeronautical nanofluid applications, nonlinear thermal radiation is becoming more important. Choi[5] and Buongiorno[6] presented fundamental nanofluid behavior insights, whereas Khan *et al*[24], Zhao-Wei Tong[25], and Hayat[26] used Cattaneo-Christov heat flux models to study magnetohydrodynamic (MHD) flows driven by nonlinear radiation. When a material is subjected to a magnetic field and an electric field, the Hall current is the flow of charge carrier's perpendicular to each other. Edwin Hall developed the Hall Effect in 1879. The Hall Effect occurs when a magnetic field deflects electrons or holes in a material, generating a voltage differential. Hall voltage is proportional to magnetic field strength and material current. Hall currents affect current density and magnetic forces in MHD generators, accelerators, and transformers. Abo-Eldahab and Salem[27], Shit[28], and Chamkha *et al*.[29] explained how Hall effects and heat radiation affect nanofluid flow. Many earlier research assumed constant viscosity. Animasahun[30] and Abd El-Aziz[31] proved that viscosity changes with temperature, which affects fluid behavior. Coriolis-induced rotating flows are crucial in space and weather science. Liaquat Ali Lund *et al*.[32] studied rotating nanofluid heat and mass transfer.

This study investigates the combined effects of activation energy, temperature-dependent viscosity, and nonlinear thermal radiation on Cu–Al_2O_3–Ag/water ternary nanofluid flow over a stretching surface, where the ternary system combining copper, alumina, and silver nanoparticles in water leverages the high thermal conductivity of copper, the stability and mechanical robustness of Al_2O_3, and the enhanced heat transfer and antimicrobial properties of silver, thereby outperforming many mono- or hybrid-nanoparticle formulations for applications in cooling systems, heat exchangers, energy storage, lubrication, and medical uses such as sterilization and targeted drug delivery. The present work introduces this ternary nanoparticle configuration to improve thermal performance compared with earlier studies that largely focused on single- or binary-nanoparticle suspensions, and the results indicate that the ternary nanofluid exhibits superior heat-transfer characteristics, offering potential for more efficient industrial cooling systems, while also highlighting the need for further investigation into different nanoparticle concentrations and their influence on flow dynamics to fully optimize the approach, with a distinguishing feature of this analysis being its integrated treatment of nonlinear thermal radiation, variable viscosity, and chemical reaction effects, a combination that has been relatively underexplored in the existing literature. When juxtaposed with mononanofluids, in which a single species of nanoparticle is dispersed in the base fluid, the ternary suspension benefits from a complementary partition of functional roles: copper supplies high lattice thermal conductivity, alumina contributes mechanical robustness and colloidal stability, and silver augments both thermal transport and antimicrobial activity. Whereas mononanofluid formulations typically offer only a modest enhancement of the effective thermal conductivity over the base fluid, and binary hybrids provide an intermediate gain, the present numerical experiments benchmarked against the limiting-case results of Shit and Haldar[28] and of Rao *et al*.[16] demonstrate that the Cu–Al_2O_3–Ag triplet consistently delivers higher local Nusselt numbers across the explored parameter space. The integrated treatment of partial slip, Arrhenius activation energy, Newtonian cooling and Hall current within a single rotating-frame formulation further differentiates the present analysis from earlier mono- and hybrid-nanofluid investigations.

To address the resulting boundary layer equations, the analysis employs a fifth-order Runge–Kutta–Fehlberg method alongside the shooting technique. The influence of key dimensionless parameters on the profiles of velocity, temperature, and nanoparticle concentration is thoroughly examined. Additionally, the variations in skin friction coefficient, Nusselt number, and Sherwood number are evaluated to offer suggestions for the system's overall heat and mass transfer behavior.

Application

Engineering systems and natural ecosystems depend on thermal and concentration buoyancy-influenced transport phenomena. Chemical distillation, heat exchangers, solar energy collection, and thermal protection systems use these processes because heat and chemical reactions drive them. Sunlight-induced thermal convection in air flows is affected by water vapor concentration. Buoyancy-driven convection from coupled heat and mass transfer in porous media is also important in energy engineering. These include moisture migration, fiber insulation, chemical pollutant dispersion in saturated soils, geothermal energy extraction, and subsurface hazardous waste disposal. Using ternary nanofluids in heat transfer can improve the efficiency, performance, and sustainability of engineering systems in several industries. Ternary nanofluids cool laptops, phones, and LED lights. Ternary nanofluids could transport heat in CSP systems. This study on flow and heat transfer past a stretching surface with variable viscosity and activation energy has many scientific and technological implications. This advances fluid flow and heat transfer science and industry. Figure 1 illustrates nanofluid industrial applications.

Novelty

The study explores the effects of a magneto-radiative water-based ($Cu + Al_2O_3 + Ag$) hybrid nanofluid on convective heat and mass transfer flow in a stretching sheet with variable viscosity, viscous dissipation, thermal radiation, Joule heating, activation energy, and a non-uniform heat source. This understanding is useful in thermal management, energy conversion, and heat exchangers.

Mathematical formulation of the model

This study investigates the steady three-dimensional free convective flow of an incompressible, viscous, and electrically conducting fluid over a stretching surface, where the stretching velocity increases linearly with distance from a fixed point. The coordinate system is defined as the x-axis along the stretching direction, the y-axis normal to the sheet, and the z-axis as the transverse direction. A uniform magnetic field ($\vec{B}$) is applied transversely, and the system experiences rotation ($\vec{\Omega}$) about the y-axis. Furthermore, the fluid's viscosity is assumed to be temperature-dependent, decreasing linearly with increasing temperature.

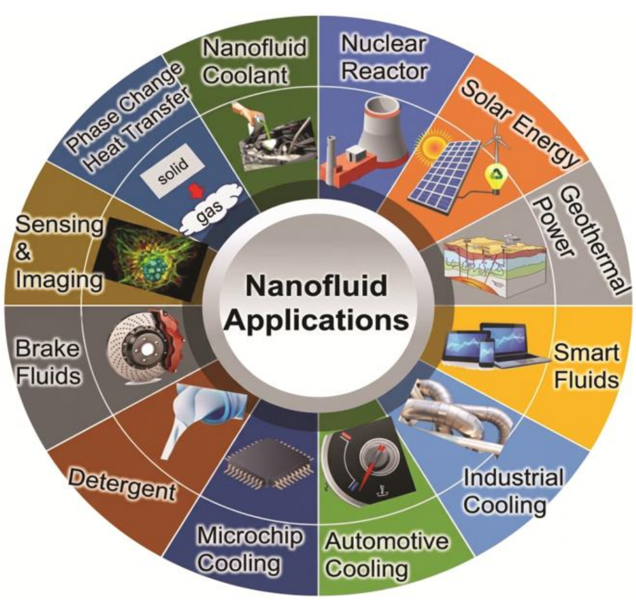

Fig. 1 — Various applications associated with nanofluids

The following assumptions form the basis of the mathematical formulation:

- The study considers steady, laminar, two-dimensional flow of a Newtonian, temperature-dependent viscosity ternary nanofluid ($Cu + Al_2O_3 + Ag$ in water) using boundary layer and Boussinesq approximations (turbulence, unsteady transients and compressibility effects, although potentially relevant in certain industrial regimes, are deliberately excluded so as to isolate the coupled influence of the physical parameters of central interest; their incorporation is reserved for subsequent investigations)
- It is assured that the base fluid (Water based) and suspended nanoparticles ($Cu+Al_2O_3$ + Ag)are in thermal equilibrium (this single-phase representation is adopted for analytical tractability; departures from local thermal equilibrium that may arise in highly dynamic regimes are acknowledged as a limitation)
- The pressure gradient is considered constant such that the pressure gradient is zero
- In order to evaluate the flow within the porous matrix, Brinkman-Foechheimer extended Darcy model is used
- Temperature dependent viscosity is considered
- A fully developed ternary nanofluid flow over a stretching sheet is considered with convective heating, thermal radiation, heat generation, and negligible induced magnetic field.
- Non-uniform heat source/sink, viscous dissipation, and Joule heating are included in the energy equation.

The model includes Brinkman–Forchheimer porous flow, Brownian motion, thermophoresis, activation energy, and temperature-dependent viscosity.

Effective Viscosity of Ternary Nanofluid μ_{thnf} is given by:

$$\mu_{thnf} = \frac{\mu_f}{A_1}, \mathrm{A}_1 = (1-\phi_1)(1-\phi_2)(1-\phi_3)]^{2.5} \quad \ldots (1)$$

where μ_f is dynamic viscosity of the base fluid, A1 accounts for the volume fractions ϕ_1,ϕ_2,ϕ_3 of three different types of nanoparticles. This formula gives the effective viscosity of a ternary hybrid nanofluid using Brinkman's model adjusted for multiple particles.

Temperature-Dependent Viscosity Model is given by:

$$\frac{1}{\mu_\infty} = a(T - T_\infty),$$

where:

- Viscosity is inversely proportional to a linear function of temperature.
- μ_∞: viscosity at ambient temperature T_∞ (taken throughout the present study as the laboratory room temperature, T_∞ = 298 K, *i.e.* 25°C).
- γ_0: thermal viscosity parameter.
- This model assumes that as temperature increases, viscosity decreases, which is typical for liquids.

Simplified Linear Model:

$$\frac{1}{\mu_\infty} = a(T - T_\infty) \qquad \ldots (2)$$

This is a rearranged form where $a = \dfrac{\gamma_0}{\mu_\infty}$ and

$$T_r = T_\infty - \frac{1}{\gamma_0}$$

Both a and T_r are determined by the thermal characteristics of the fluid, especially the parameter γ_0. γ_0 >0 applies to liquids (viscosity decreases with heat) where as γ_0<0 applies to gases (viscosity may increase with temperature). The model ensures realistic fluid behavior in thermally driven flow problems, especially for complex fluids like nanofluids. Meanwhile, a>0 corresponds to liquids, while a < 0 applies to gases (Table 1).

The boundary layer free-convective flow with mass transfer, considering generalized Ohm's law and the effect of Hall currents, is governed by the following system of equations:

$$\frac{\partial u}{\partial x} + \frac{\partial v}{\partial y} = 0 \qquad \ldots (3)$$

Table 1 — Thermophysical characteristics of nanoparticles[33]

Nanofluid particles				Base fluid
	Cu	Al_2O_3	Ag	Water
Density (ρ), kg/m³	8933	3970	5180	997.1
Specific heat Capacity (Cp) J kg^{-1} K^{-1}	385	765	670	4179
Thermal conductivity (kf). W m^{-1} K^{-1}	400	40	9.7	0.6071
B × $10^{-5}K^{-1}$	1.67	0.85	0.5	21
σ(sm^{-1})	5.96 × 10^7	1.0 × 10^{-10}	6.3 × 107	5.5 × 10^{-6}

$$\rho_{thnf}\left(u\frac{\partial u}{\partial x} + v\frac{\partial u}{\partial y}\right) = \mu_{thnf}\frac{\partial^2 u}{\partial y^2} - (\frac{\mu_{thnf}}{k_p})u - (\frac{C_b}{\sqrt{k_p}})\mathrm{u}^2 - 2\Omega w$$
$$+ g(1-C_\infty)(\rho_f\beta)_{thnf}\,g(T-T_\infty) - (\rho_p - \rho_{f_\infty})kg(C - C_\infty) - \frac{\sigma_{thn\,f}B_0^2}{1+m^2}(u + mw) \qquad \ldots (4)$$

$$\rho_{thnf}\left(u\frac{\partial w}{\partial x} + v\frac{\partial w}{\partial y}\right) = \mu_{thnf}\frac{\partial^2 w}{\partial y^2} - (\frac{\mu_{thnf}}{k_p})\mathrm{w} + 2\Omega u - (\frac{C_b}{\sqrt{k_p}})\mathrm{w}^2 + \frac{\sigma_{thn\,f}B_0^2}{1+m^2}(mu - w) \qquad \ldots (5)$$

$$(\rho C_p)_{thnf}\left(u\frac{\partial T}{\partial x} + v\frac{\partial T}{\partial y}\right) = k_{thnf}\frac{\partial^2 T}{\partial y^2} + \tau\{D_B(\frac{\partial T}{\partial x}\frac{\partial C}{\partial x} + \frac{\partial T}{\partial y}\frac{\partial C}{\partial y}) + \frac{D_T}{T_\infty}((\frac{\partial T}{\partial x})^2 + (\frac{\partial T}{\partial y})^2)]$$
$$-\frac{\partial(q_r)}{\partial y} + (A_{11}^{'}(T_w - T_\infty)u + B_{11}^{'}(T - T_\infty)) + 2\mu_{thnf}((\frac{\partial u}{\partial y})^2 + (\frac{\partial w}{\partial y})^2) + \sigma_{thnf}\mu_e^2 H_o^2(u^2 + w^2) \qquad \ldots (6)$$

$$u\frac{\partial C}{\partial x} + v\frac{\partial C}{\partial y} = D_B\frac{\partial^2 C}{\partial y^2} - k_0\left(C - C_\infty\right)(\frac{T}{T_\infty})^n Exp(-\frac{E_a}{KT}) + \frac{D_T}{T_\infty}\frac{\partial^2 T}{\partial y^2} \qquad \ldots (7)$$

The boundary conditions for the present problem can be written as

$$u = bx + A_{33}^{'}\frac{\partial u}{\partial y},\ v = w = 0, \quad -k_{thnf}\frac{\partial T}{\partial y} = h_f(Tw - T),$$
$$C = C_w \text{ at } y=0 \qquad \ldots (8)$$

$$u \to 0,\ w \to 0,\ T \to T_\infty,\ C \to C_\infty \text{at} y \to \infty \qquad \ldots (9)$$

The boundary conditions describe how the fluid behaves at the surface of the stretching sheet (y=0) and far away from it (y→∞) for a heat and mass transfer problem involving MHD flow over a stretching surface.

At y=0:

- $u = bx + A_{33}^{'}\dfrac{\partial u}{\partial y}$: The tangential velocity at the surface is influenced by both stretching of the sheet (through bx) and a slip condition represented by the term involving A33, which is the velocity slip parameter.

- $v=w=0$: The normal (vertical) velocity components are zero, meaning there is no fluid penetration through the surface.
- $-k_{thnf}\dfrac{\partial T}{\partial y}=h_f(Tw-T)$: A convective boundary condition representing heat transfer between the fluid and a hot surface.
- $C = C_w$: The concentration of the solute (nanoparticles or chemical species) at the wall is C_w.

As $y\to\infty$ (far from the surface):

- $u\to 0$, $w\to 0$: The fluid is stationary far from the surface; both horizontal and vertical velocity components vanish.
- $T\to T_\infty$: The temperature approaches the ambient fluid temperature.
- $C\to C_\infty$: The concentration tends to the ambient concentration.

By Rosseland approximation, we have:

$$q_r=-\frac{4\sigma^{\bullet}}{3\beta_R}\frac{\partial T'^4}{\partial y} \quad \dots (10)$$

$$T'^4\cong 4TT_\infty^3-3T_\infty^4 \quad \dots (11)$$

where $\sigma^{\bullet}$ is the Stefan –Boltzman constant and β_R is the mean absorption constant.

The non-dimensional temperature $\theta(\eta)=\dfrac{T-T_\infty}{T_w-T_\infty}$ can be simplified as

$$T=T_\infty(1+(\theta_w-1)\theta) \quad \dots (12)$$

where $\theta=\dfrac{T_w}{T_\infty}$ is the temperature parameter.

Ternary hybrid nanofluid[33]

Density(ρ), Kg/m^3	$(\rho)_{thnf}=(1-\phi_1)[(1-\phi_2)[(1-\phi_3)+\phi_3\frac{\rho_3}{\rho_f}]+\phi_2\frac{\rho_2}{\rho_f}]+\phi_1\frac{\rho_1}{\rho_f}$
Viscosity (μ) N s/m^2	$\mu_{thnf}=[(1-\phi_1)]^{-2.5}[(1-\phi_2)]^{-2.5}[(1-\phi_3)]^{-2.5}$
Specific heat Capacity (Cp)J/k	$(\rho C_p)_{thnf}=(1-\phi_1)[(1-\phi_2)[(1-\phi_3)+\phi_3\frac{(\rho C_p)_3}{(\rho C_p)_f}]+\phi_2\frac{(\rho C_p)_2}{(\rho C_p)_f}]+\phi_1\frac{(\rho C_p)_1}{(\rho C_p)_f}$
Thermal conductivity (kf). W/m-k	$\frac{k_{thnf}}{k_{hnf}}=\frac{k_1+2k_{hnf}-2\phi_2(\mathrm{k}_{hnf}-k_f)}{k_1+2k_{hnf}+\phi_2(\mathrm{k}_{hnf}-k_f)},\frac{k_{hnf}}{k_{nf}}=\frac{k_3+2k_{nf}-2\phi_3(\mathrm{k}_{nf}-k_f)}{k_3+2k_{nf}+\phi_3(\mathrm{k}_{nf}-k_f)},$ $\frac{k_{nf}}{k_f}=\frac{k_3+2k_f-2\phi_3(\mathrm{k}_f-k_3)}{k_3+2k_f+\phi_3(\mathrm{k}_f-k_3)},$
Thermal diffusivity (β × 10^{-5} (K^{-1})	$(\rho\beta)_{thnf}=(1-\phi_1)[(1-\phi_2)[(1-\phi_3)+\phi_3\frac{(\rho\beta)_3}{(\rho\beta)_f}]+\phi_2\frac{(\rho\beta)_2}{(\rho\beta)_f}]+\phi_1\frac{(\rho\beta)_1}{(\rho\beta)_f}$
Electrical conductivity (σ(s/m)	$\frac{\sigma_{thnf}}{\sigma_{hnf}}=\frac{\sigma_1(1+2\phi_1)+\sigma_{hnf}(1-2\varphi_1)}{\sigma_1(1-\phi_1)+\sigma_{hnf}(1+\phi_1)},\frac{\sigma_{hnf}}{\sigma_{nf}}=\frac{\sigma_2(1+2\phi_2)+\sigma_{nf}(1-2\varphi_2)}{\sigma_2(1-\phi_2)+\sigma_{nf}(1+\phi_2)},$ $\frac{\sigma_{nf}}{\sigma_f}=\frac{\sigma_3(1+2\phi_3)+\sigma_f(1-2\varphi_3)}{\sigma_3(1-\phi_3)+\sigma_f(1+\phi_3)}$

To analyze the flow behavior in the region near the stretching surface, the following similarity transformations are introduced.

$$u=bxf'(\eta);v=-\sqrt{bv}f(\eta);w=bxg(\eta);$$
$$\eta=\sqrt{\frac{b}{v}}y;\theta(\eta)=\frac{T-T_\infty}{T_w-T_\infty};\Phi=\frac{C-C_\infty}{C_w-C_\infty} \quad \dots (13)$$

Clearly, the continuity Eq. (3) is satisfied by *u* and *v* defined in Eq. (9), Substituting Eq. (10) the Eqs. (4-7) reduce to:

$$\left(\frac{\theta-\theta_r}{\theta_r}\right)\mathrm{A}_1\mathrm{A}_2(f'^2-f\ \ f'')+f'''-\left(\frac{\theta'}{\theta-\theta_r}\right)f''+2A_1R.g.\left(\frac{\theta-\theta_r}{\theta_r}\right)GA_4A_1(\theta-N\varphi)-\mathrm{K}\mathrm{f}'$$
$$-A_1\,\mathrm{fs(f')}^2+M^2A_1A_6\left(\frac{\theta'-\theta_r}{\theta_r}\right)\left(\frac{f'+mg}{1+m^2}\right)=0 \quad \dots (14)$$

$$\left(\frac{\theta-\theta_r}{\theta_r}\right)\mathrm{A}_1.\mathrm{A}_2(f'g-fg')+g''-\left(\frac{\theta'}{\theta-\theta_r}\right)g'-2A_1.R.f'-K.g-A_1.fs.g$$
$$+M^2A_1.A_6\left(\frac{\theta-\theta_r}{\theta_r}\right)\left(\frac{mf'+g}{1+m^2}\right)=0 \quad \dots (15)$$

$$Rd((1+(\theta_w-1)\theta)^3)\theta')'+Nb(\frac{\partial\theta}{\partial\eta}\frac{\partial\varphi}{\partial\eta})+Nt(\frac{\partial\theta}{\partial\eta})^2+A_{11}\,\mathrm{f}'+B_{11}\theta+Ec\,\mathrm{Pr}((f'')^2$$
$$+(g')^2)+\frac{Ec\,\mathrm{Pr}\,M^2A_6}{1+m^2}(\mathrm{f}'^2+\mathrm{g}^2)=0 \quad \dots (16)$$

$$\frac{1}{Le}\varphi''-(f\varphi'-\gamma.\varphi.(1+n\delta\theta)\,\mathrm{Exp}(-\frac{E_1}{1+\delta\theta}))+(\frac{Nt}{Nb})(\theta'')=0 \quad \dots (17)$$

transformed boundary conditions are given by:

$f'(\eta)=1+A_{33}f''(\eta), f(\eta)=0,$

$g(\eta)=0, \theta'(\eta)=-h1(1-\theta), \varphi(\eta)=1$ at $\eta=0$ … (18)

$f'(\eta)\to 0, g(\eta)\to 0, \theta(\eta)\to 0, \varphi(\eta)\to 0$ at $\eta\to\infty$ … (19)

where a prime denotes the differentiation with respect to η only and the dimensionless parameters appearing in the Eqs. (13)-(17) are respectively defined as $\theta_r=\dfrac{T_r-T_\infty}{T_w-T_\infty}=-\left[\dfrac{1}{\gamma_0(T_w-T_\infty)}\right]$ the viscosity parameter, $M=\dfrac{\sigma B_0^2}{P_\infty b}$ the magnetic parameter,

$\Pr = \frac{\rho C_p \nu}{k_f}$ the Prandtl number, $\gamma = \frac{k_0}{b}(C_w - C_\infty)$ the non-dimensional chemical reaction parameter, $G = \frac{g_0 \beta\ (T_w - T_\infty)}{b^2 x}$ the local Grashof number, $N = \frac{(\rho_p - \rho_{f\infty})(C_w - C_\infty)}{\rho_{f\infty}(1 - C_\infty)(T_w - T_\infty)}$ the Buoyancy ratio, $Rd = \frac{4T_\infty{}^3 \sigma^*}{k_f \beta_R}$ the thermal radiation parameter, $Le = \frac{\mu_f}{\rho_\infty D_m}$ the Lewis number, $N_b = \frac{\tau D_B (C_w - C_\infty)}{a}$ Brownian motion parameter, $N_t = \frac{\tau D_T (T_w - T_\infty)}{a T_\infty}$ Thermophoresis parameter. $h_1 = (\frac{h_f}{k_f})\sqrt{\frac{\nu}{b}}$ is convective heat transfer constant. $E_1 = \frac{E_a}{KT_\infty}$ is the activation energy parameter, $A = \theta_w = \frac{T}{T_w}, \delta = A - 1$ is the temperature difference ratio, $fs = F\sqrt{K_p}$ is the inertia parameter or Forchheimer number, R=2Ω/b is rotation parameter and K= $\nu/k_p b$ is porosity parameter.

$$\mathrm{A}_1 = (1-\phi_1)(1-\phi_2)(1-\phi_3)]^{2.5}$$

$$\mathrm{A}_2 = [(1-\phi_1)(1-\phi_{s_1} + \frac{\rho_{s1}}{\rho_f}\phi_1) + \frac{\rho_{s2}}{\rho_f}\phi_2] + \frac{\rho_{s3}}{\rho_f}\phi_3$$

$$\mathrm{A}_3 = [(1-\phi_1)(1-\phi_{s_1} + \frac{\beta_{s1}}{\beta_f}\phi_1) + \frac{\beta_{s2}}{\beta_f}\phi_2] + \frac{\beta_{s3}}{\beta_f}\phi_3$$

$$\mathrm{A}_4 = (1-\phi_3)[(1-\phi_2)(1-\phi_1 + \frac{(\rho C_p)_{s1}}{(\rho C_p)_f}\phi_1) \cdot$$

$$+ \frac{(\rho C_p)_{s1}}{(\rho C_p)_f}\phi_1) + \frac{(\rho C_p)_{s2}}{(\rho C_p)_f}\phi_2] + \frac{(\rho C_p)_{s3}}{(\rho C_p)_f}\phi_3$$

$$A_5 = \frac{k_{s3} + 2k_{hnf} - 2\phi_3(\mathrm{k}_{hnf} - k_{s3})}{k_{s3} + 2k_{hnf} + \phi_3(\mathrm{k}_{hnf} - k_{s3})},$$

$$A_6 = \frac{\sigma_{s3} + 2\sigma_{hnf} - 2\phi_3(\sigma_{hnf} - \sigma_{s3})}{\sigma_{s3} + 2\sigma_{hnf} + \phi_3(\sigma_{hnf} - \sigma_{s3})}$$

Solution Procedure

The coupled non-linear ODEs (13)-(17), with third-order f equation and second-order g, θ, and ϕ equations, are reduced to first-order equations. We use the shooting approach to estimate missing initial values at η=0. The effectiveness of this strategy relies on choosing a finite value for η∞.

Start by guessing η∞ and solve the boundary value problem to determine f′′, g', θ′, and ϕ′. The method is continued with greater η∞ values until the desired precision is achieved. After getting all initial values, the fifth-order Runge-Kutta-Fehlberg technique with automatic grid modification solves the problem for improved precision and faster convergence. Physical parameters include Grashof number, magnetic field, rotation, Hall current, activation energy, Prandtl number, radiation, Lewis number, heat source, chemical reaction rate, and convective heat transfer coefficient affect the selection of η∞. These are carefully selected to avoid numerical instability. The shot error was kept below 10^{-6} during the solution process.

The local skin-friction coefficient C_f, the local Nusselt number *Nu* and the local Sherwood number *Sh* defined by

$$C_{fx} = \frac{\tau_w}{\mu b x \sqrt{\frac{b}{\nu}}} = f''(0), C_{f_z} = g'(0) \quad \ldots (20)$$

where

$$\tau_w = \mu\left(\frac{\partial u}{\partial y}\right)_{y=0} = \mu b x \sqrt{\tfrac{b}{\nu}} f''(0), Nu = \frac{\dot{q}_w}{k_f \sqrt{\frac{b}{\nu}}(T_w - T_\infty)} \quad \ldots (21)$$

where

$$q_w = -k_f\left(\frac{\partial T}{\partial y}\right)_{y=0} = -k_f \sqrt{\tfrac{b}{\nu}}(T_w - T_\infty)\theta'(0)$$

and

$$Sh = \frac{m_w}{D_m \sqrt{\frac{b}{\nu}}(C_w - C_\infty)} = -\Phi'(0)$$

where

$$m_w = -D_m\left(\frac{\partial C}{\partial y}\right)_{y=0} = -D_m \sqrt{\tfrac{b}{\nu}}(C_w - C_\infty)\Phi'(0)$$

The results obtained in the present study have been validated by comparing them with the previously published findings of Shit and Haldar[28], as shown in (Table 2a), and show excellent agreement**.**

In the absence of rotation (R = 0), Hall effects (m = 0), nonlinear thermal radiation (A = 0), activation energy (E_1 = 0), temperature difference ratio (δ = 0), index number (n = 0), and variable viscosity (θ_r = 0), the present results show good agreement with those reported by Rao *et al*[16] (Table 2b).

Results and Discussion

This study investigates the influence of variable viscosity (θr), non-linear thermal radiation (A), activation energy (E_1), partial slip (A_{33}), and non-uniform heat source parameters (A_{11}, B_{11}) on the rotating hydromagnetic non-Darcy convective heat and mass transfer flow of water-based ternary nanofluids (Cu + Al_2O_3 + Ag/water) and hybrid nanofluids (Al_2O_3 + Ag/water) past a stretching sheet, subject to convective boundary conditions.

The effect of the parameters on both axial and secondary velocities is illustrated in the following figures

Figures 2a-2b illustrate the variations of axial velocity (f′) and secondary velocity (g) with respect to the nanoparticle volume fraction (ϕ). An increase in leads to a reduction in both axial and secondary velocities throughout the flow domain. The axial velocity in water-based ternary nanofluids is significantly higher than that in hybrid nanofluids, whereas the secondary velocity exhibits the opposite trend (Fig. 2a).

Figures 3a-3d indicate that the Hall parameter (m), Forchheimer parameter (fs), Brownian motion

Table 2a — Comparison of Nu and Sh at η=0 at R=0, h1=0, Nb=Nt=0, E1=0,δ=0, ϕ1=ϕ2=ϕ3=0

M	Rd	γ	θr	*Shit and Haldar*[28]		Present Results	
				$-\theta'(0)$	$-\phi'(0)$	Nu (0)	Sh (0)
0.5	1	0.5	-2	0.51857	0.6195	-0.51889	0.61955
0.5	1	1.5	-2	0.6956	1.0959	-0.69569	1.09599
0.5	1	0.5	-4	0.5974	0.4071	-0.59745	0.40722
0.5	1	0.5	-6	0.6969	0.6253	-0.69679	0.62534

Table 2b — Comparison of $-\theta'(0)$ and $-\phi'(0)$ at η=0 with at R=m=A=E1=δ=n=θ_r=0

G	M	Q	fs	Rd	Ec	ϕ	A33	h1	Sc	γ	Rao et.al.[16]		Present results	
											Nu (0)	Sh (0)	Nu (0)	Sh(0)
2	0.5	0.5	0.1	0.5	0.05	0.01	0.1	0.2	0.24	0.5	0.0745348	1.10843	0.0745460	1.10854
4											0.0748758	1.11052	0.0748628	1.11052
6											0.0742124	1.10692	0.0742131	1.10701
	1.0										0.073889	1.10484	0.073891	1.10482
	1.5										0.0745928	1.10904	0.0745924	1.10912
		1.0									0.0752126	1.11082	0.0752125	1.11095
		1.5									0.1268788	1.126754	0.1268791	1.126724
			0.3								0.131249	1.142482	0.131222	1.142483
			0.5								0.0830168	1.10643	0.0830142	1.10644
				1.5							0.094189	1.09843	0.094171	1.09847
				5.0							0.0627972	1.09678	0.0627968	1.09644
					0.1						0.059865	1.079845	0.059861	1.079861
					0.15						0.0848028	1.10589	0.0848022	1.10561
						0.03					0.088149	1.09867	0.088137	1.09824
						0.05					0.0901011	1.06809	0.0901012	1.06818
							0.2				0.091428	1.04925	0.091424	1.04921
							0.3				0.193397	1.108432	0.193403	1.108436
								0.4			0.214889	1.12042	0.214891	1.12045
								0.6			0.214892	1.32968	0.214894	1.32972
									0.66		0.0832427	1.34109	0.0832435	1.34112
									1.33		0.088129	1.12456	0.088124	1.12454
										1.0	0.0914125	1.13896	0.0914121	1.13845
										1.5	0.108912	1.14621	0.108911	1.14628

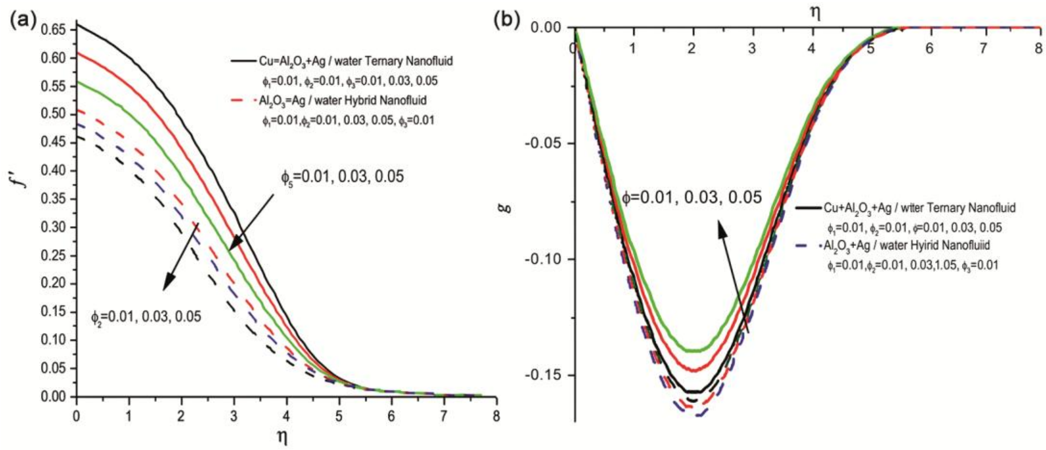

Fig. 2 — (a & b) Variation of velocity profiles f′ and induced velocity profiles g for G=2, M=0.5, m=0.5, R=0.5, fs=0.1, A=1.05, N=0.1, Rd=0.5, Ec=0.05, A33=0.1, h1=0.2, A11=0.1, B11=0.3, qr=−2, Sc=0.24, g=0.5, Q1=0.5, Nb=0.1, Nt=0.1, E1=0.2, δ=0.1, n=0.2, and Pr=0.71

parameter (Nb), and thermophoresis parameter (Nt) enhance axial velocity (f′). Because these parameters increase fluid momentum and heat diffusion, fluid motion is promoted. Figures 3e-3i demonstrate that axial velocity (f′) decreases with higher Grashof number (G), magnetic parameter (M), buoyancy ratio (N), slip parameter (A_{33}), and viscosity parameter (θr). The flow is slowed down by magnetic damping, rotational resistance, and an increase in fluid thickness. Due to its improved thermal conductivity and energy transmission, the water-based ternary nanofluid always has a higher axial velocity than the hybrid nanofluid.

Higher Hall parameters (m), rotation parameters (R), Forchheimer parameters (fs), viscosity parameters(R) Brownian motion, and thermophoresis parameters (Nb/Nt) increase secondary velocity (g) (Figs. 4a-4f).

As seen in Figures 4a-4f, the secondary velocity component g(η) rises with increasing Hall, rotation, Forchheimer, viscosity, Brownian motion, and thermophoresis parameters. The secondary flow is intensified by cross-flow effects, rotating forces, and nanoparticle-induced momentum diffusion. Due to its superior thermal and momentum transfer capabilities, the ternary nanofluid has higher secondary velocity than the hybrid nanofluid, but it decays with higher Grashof number (G)/magnetic parameter (M) values (Figs. 5a-5b). Figure 5c shows that g in a water-based ternary nanofluid is bigger than that in a water-based hybrid nanofluid in the flow zone (0,2) but less in the region (2,6) when the slip parameter (A_{33}) increases.

Parameter impact on temperature distribution

Figures 6a-6e show the temperature distribution profile θ(η) for different thermophysical parameters. Increased nanoparticle volume fraction (ϕ), thermal radiation (Rd), Eckert number (Ec), space- and temperature-dependent heat source parameters (A_{11}, B_{11}), viscosity (θr), radiation absorption (Q_1), Brownian motion (Nb), thermophoresis (Nt), and activation energy (E_1) significantly impact thermal boundary layer behavior. The temperature distribution in ternary and hybrid nanofluid flows is improved by these factors (Figs. 7a-7c).

Effect of parameters on nanoconcentration distribution

Figures 8a–9g show that energy- and diffusion-related parameters impact nanoconcentration in ternary and hybrid nanofluids oppositely. Eckert number (Ec) and Brownian motion parameter (Nb) increase nanoconcentration, indicating heat energy and microscopic agitation improve particle dispersion. Conversely, characteristics like ϕ, Grashof number, θr, γ, Nt, E1, and Pr increase mass transport resistance, reducing concentration. Prior studies have not concurrently demonstrated thermal enhancement and reactive-diffusive suppression, which show intricate interaction of physical factors affecting mass transport in multi-nanoparticle suspensions.

Variation of Stress components(τ_x,τ_z)

Variations in skin friction components τ_x and τ_z, indicating wall tangential stress (η=0), are shown in (Figs. 10-13) for various parameter influences. Figure 10 shows that a higher Grashof number (G) leads to higher τ_x and lower τ_z. Increased magnetic, viscosity, and buoyancy parameters (M, B, N) lower τ_x in water-based hybrid nanofluids but raise it in ternary nanofluids, resulting in a drop in τ_z. As shown in Figures 11 and 12, larger Hall current (m),

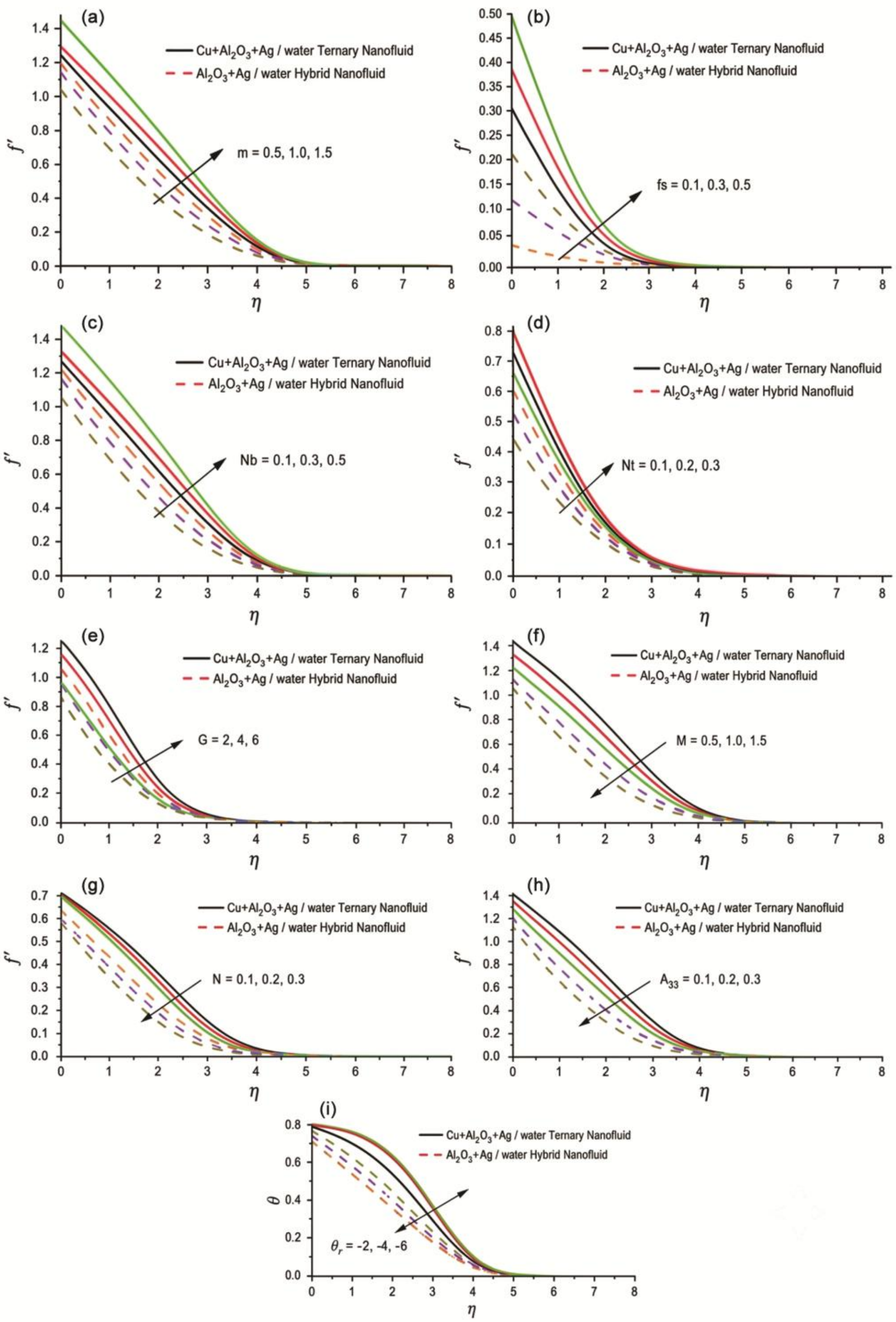

Fig. 3 — Impact of (a) m; (b) fs; (c) Nb; (d) Nt; (e) G; (f) M; (g) N; (h) A33; and (i) θr on the velocity profile f′

Forchheimer (fs), slip (A_{33}), space- and temperature-dependent heat source parameters (A_{11}, B_{11}), radiation (Rd), and Eckert number (Ec) increase both skin friction components. Increasing the viscosity parameter (θ_r) decreases τx but increases τz in ternary and hybrid nanofluids. In Figure 13, τ_x reduces with increasing nanoparticle volume fraction (ϕ), temperature ratio parameter (A), and Prandtl number (Pr), while τ_z drops in ternary nanofluids but grows in hybrids.

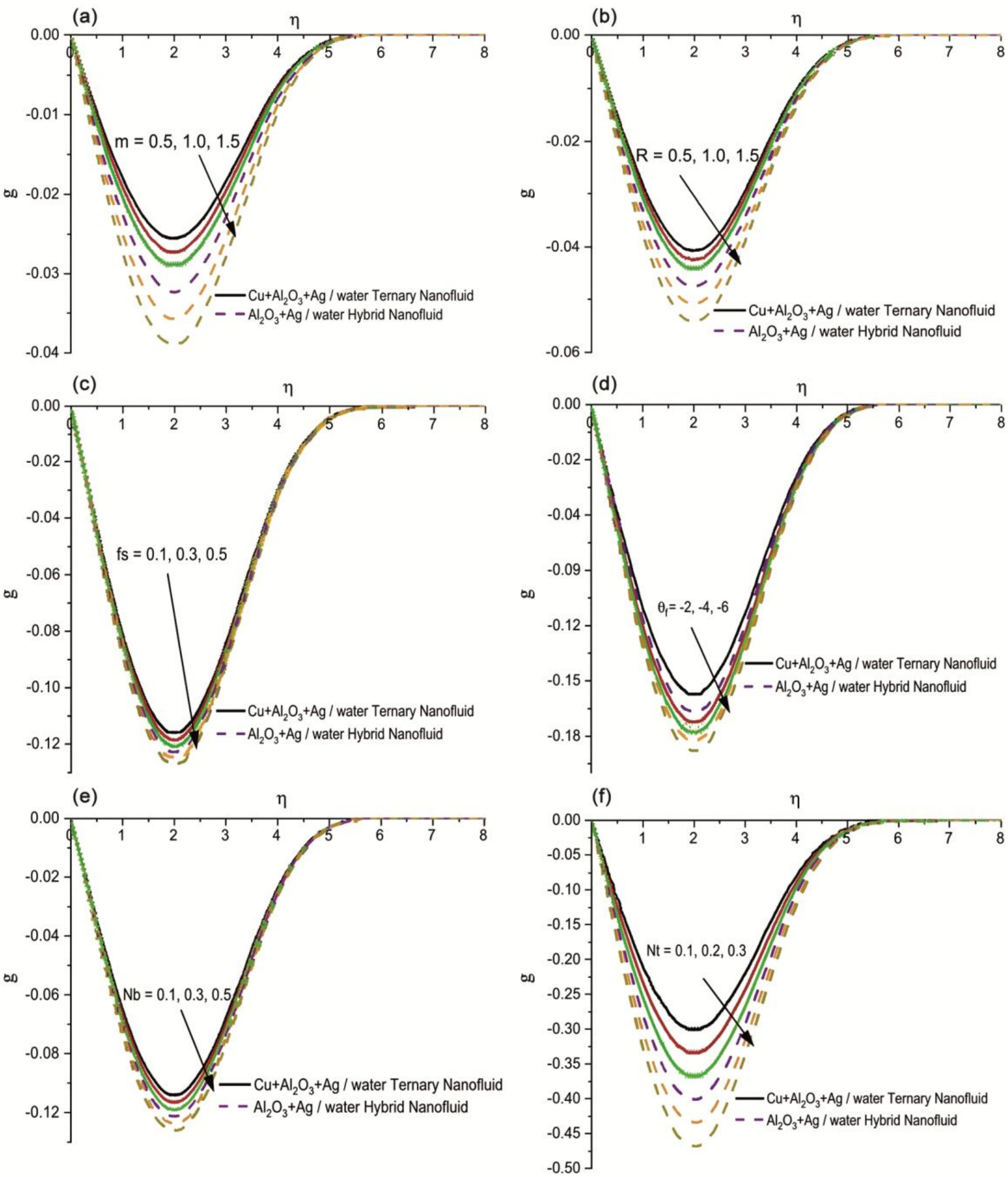

Fig. 4 — Impact of (a) m; (b) R; (c) fs; (d) θr; (e) Nb; and (f) Nt on the induced velocity profile g

Effect of parameters on Nusselt number (Nu)

Figures 14-16 show how physical characteristics affect the Nusselt number (Nu), which measures heat transport at the wall (η=0). Increasing Brownian motion parameters (Nb), nanoparticle volume fraction (ϕ), Prandtl number (Pr), slip parameter (A33), and space- and temperature-dependent heat source parameters (A_{11}, B_{11}) decrease Nu in water-based and hybrid nanofluids. However, Nu rises with increasing values of Nt, Hall, rotation, magnetic activation energy, temperature difference ratio, and index number. Additionally, the thermal radiation parameter (Rd) decreases Nu in hybrid nanofluids but increases it in ternary ones. Additionally, the radiation absorption characteristic (Q_1) decreases heat transport across both nanofluid types.

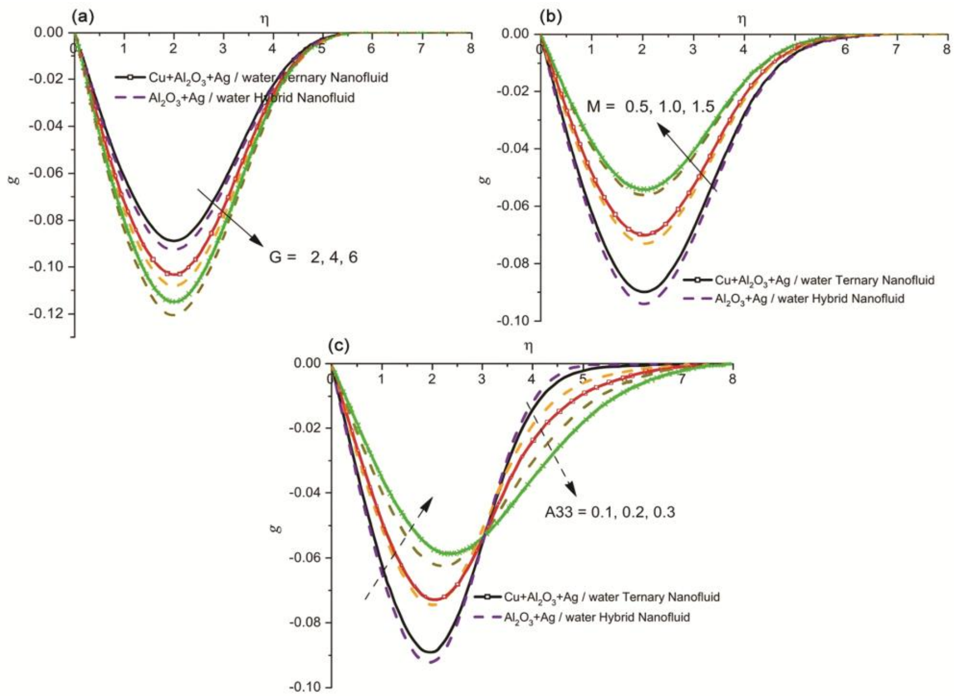

Fig. 5 — Impact of (a) G; (b) M; and (c) A33 on the induced velocity profile g

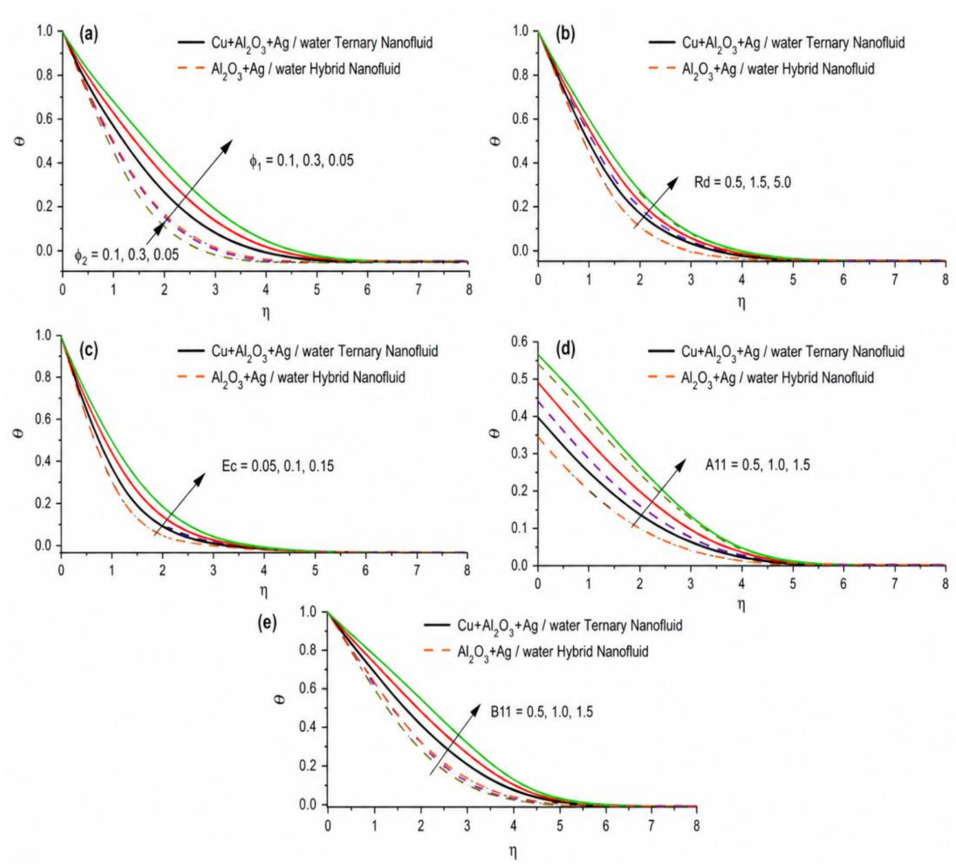

Fig. 6 — Impact of (a) ϕ; (b) Rd; (c) Ec; (d) A11; and (e) B11 on the temperature profile θ

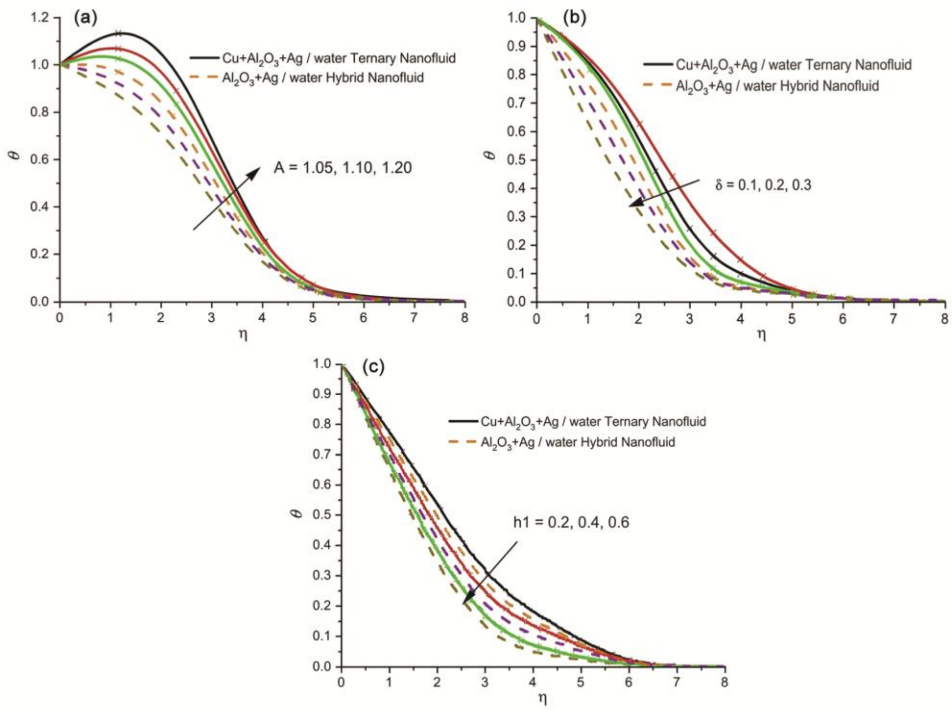

Fig. 7 — Impact of (a) A; (b) δ; and (c) h1 on the temperature profile θ

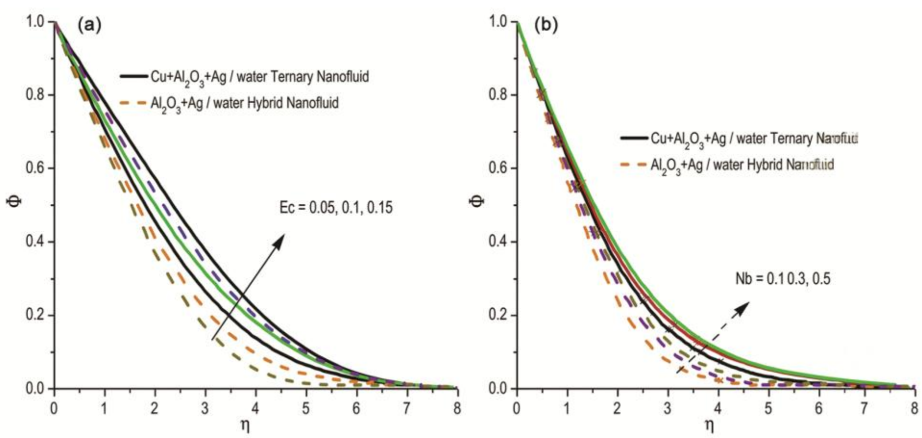

Fig. 8 — Impact of (a) Ec; and (b) Nb on the nanoparticle concentration profile Φ

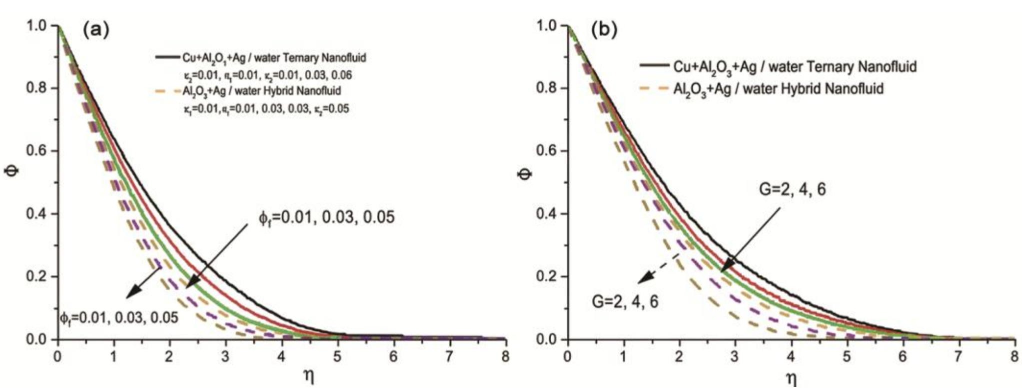

Fig. 9 — Impact of (a); G and (b) ϕ on the nanoparticle concentration profile Φ (*Contd.*)

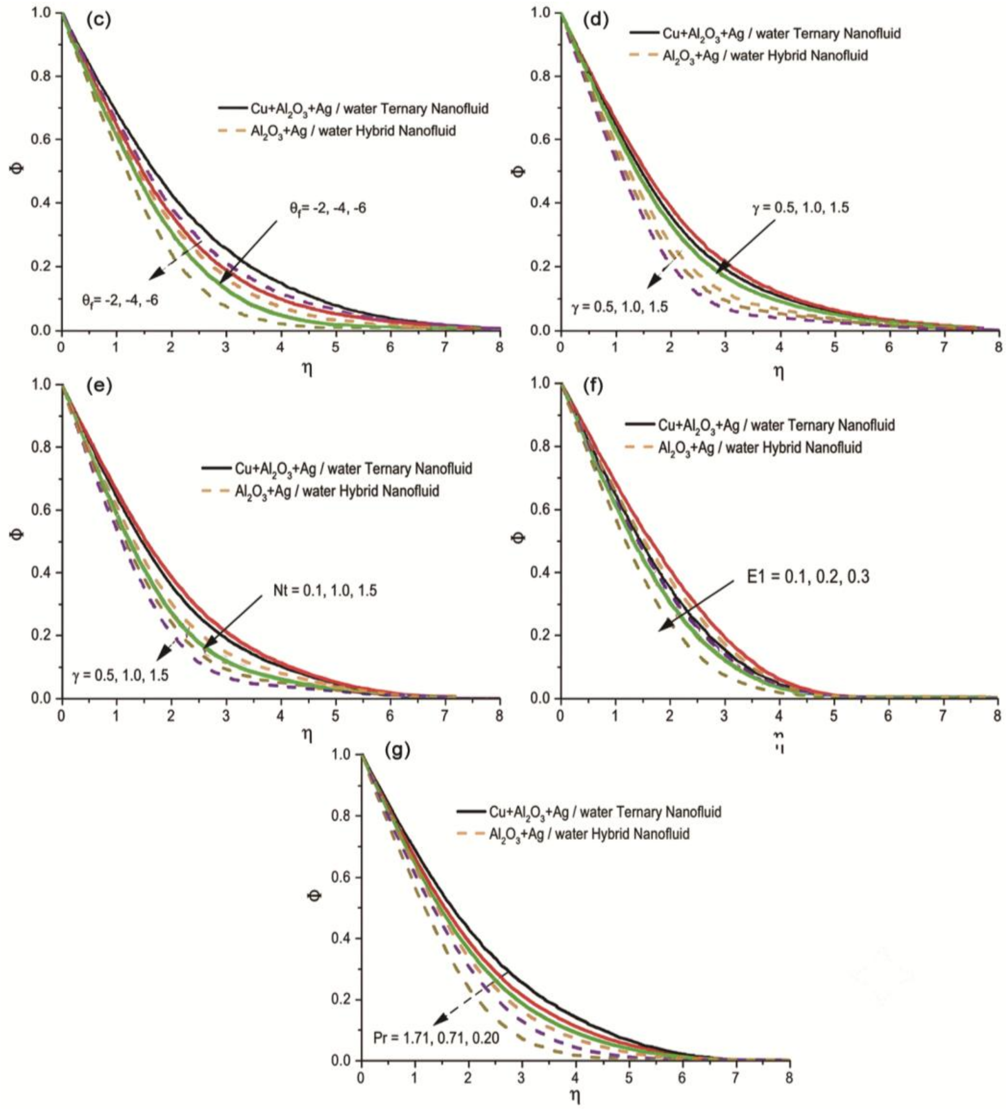

Fig. 9 — Impact of (a) G; and (b) ϕ on the nanoparticle concentration profile Φ (*Contd*.)

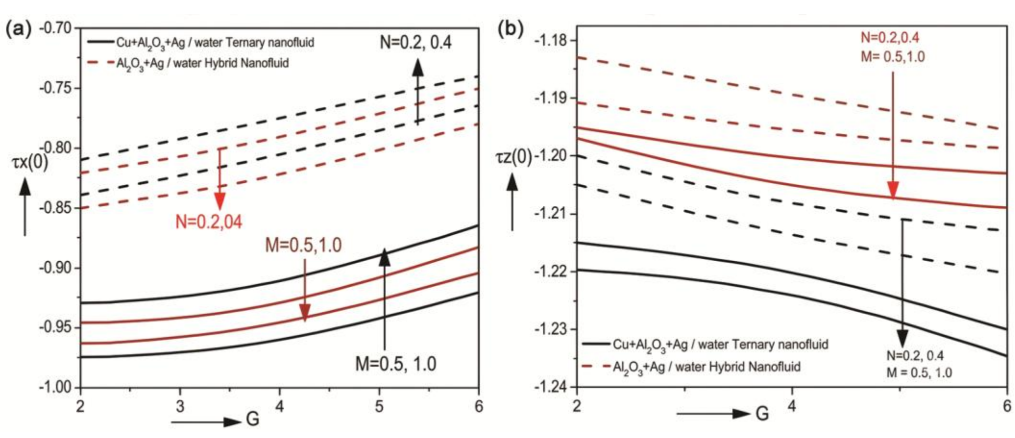

Fig. 10 — Variation of shear stress (τx,τz) at η=0 with G, M, and N

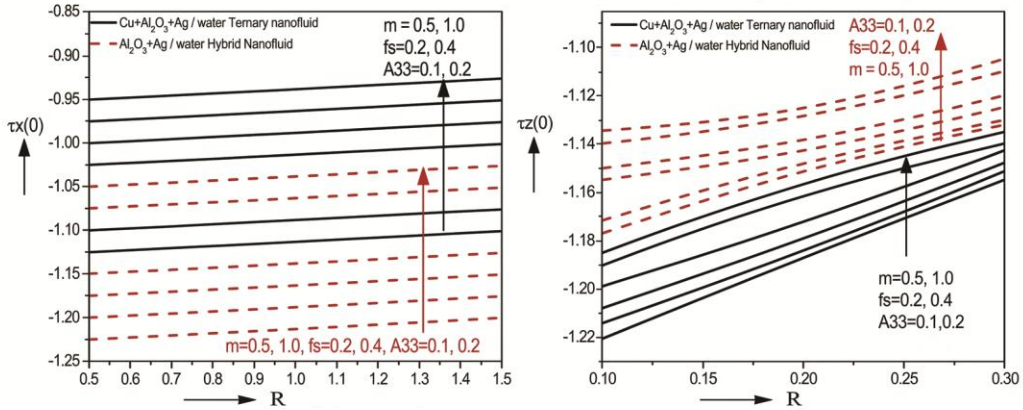

Fig. 11 — Variation of shear stress (τx,τz) at η=0 with R, m, fs, and A33

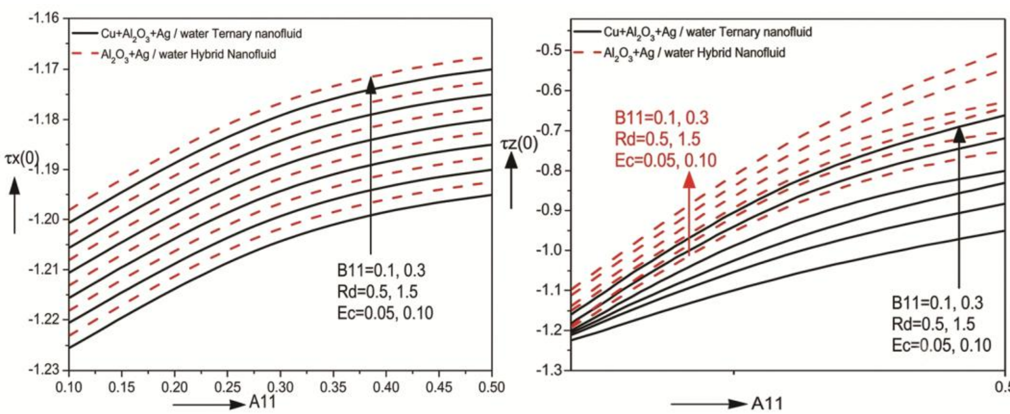

Fig. 12 — Variation of shear stress (τx,τz) at η=0 with A11, B11, R, and Ec

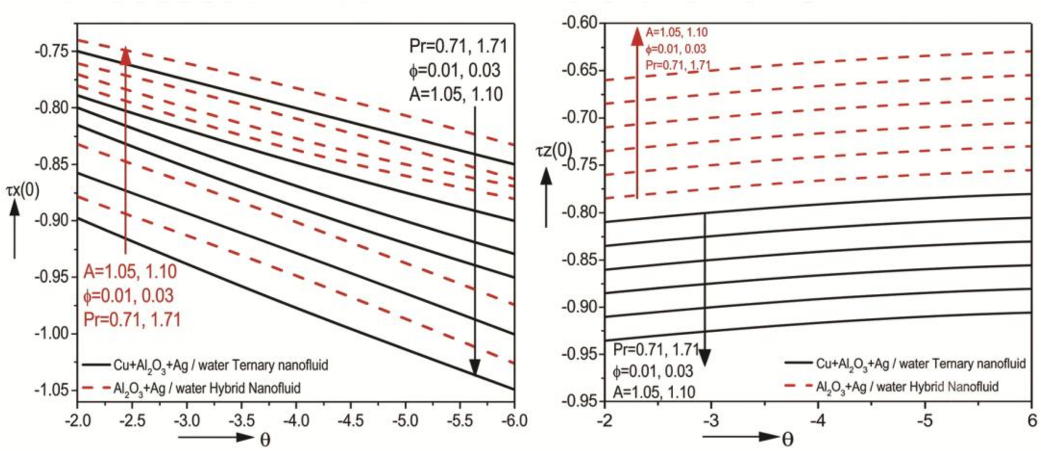

Fig. 13 — Variation of shear stress (τx,τz) at η=0 with (a) θr, Pr, A, ϕ; and (b) ϕ, Pr, A33, and B

Effect of parameters on Sherwood number (Sh)

Figures 17-18 show how different parameters affect the Sherwood number (Sh), which measures mass transfer at the wall (η=0). Sh increases with increasing Rd, A11, B11, and Ec in water-based ternary and hybrid nanofluids (Fig. 17). Increased Brownian motion parameters (Nb), thermophoresis parameter (Nt), Prandtl number (Pr), and nanoparticle volume fraction (ϕ) further improve Sh (Fig. 18). In contrast, Sh declines with increasing Schmidt number (Sc), viscosity (θr), slip (A33), and nonlinear thermal radiation (A) (Fig. 18). According to Figure 18, Sh

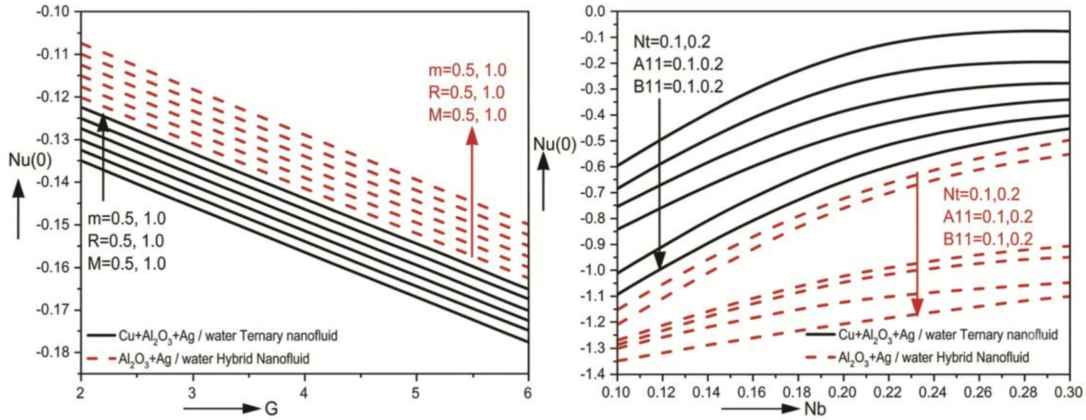

Fig. 14 — Variation of Nusselt number (Nu) at η=0 with (a) G, m, R, M; and (b) Nb, Nt, A11, and B11

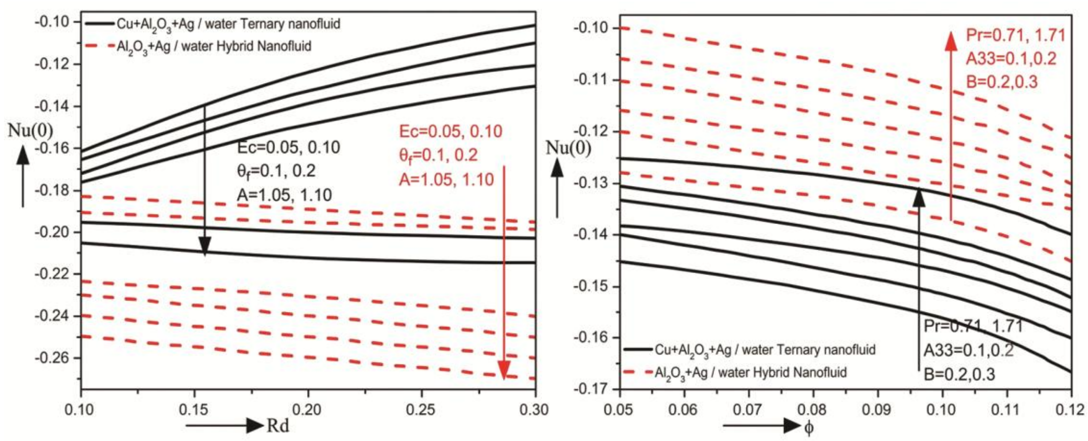

Fig. 15 — Variation of Nusselt number (Nu) at η=0 with (a) Rd, Ec, θr, A; and (b) ϕ, Pr, A33, and B

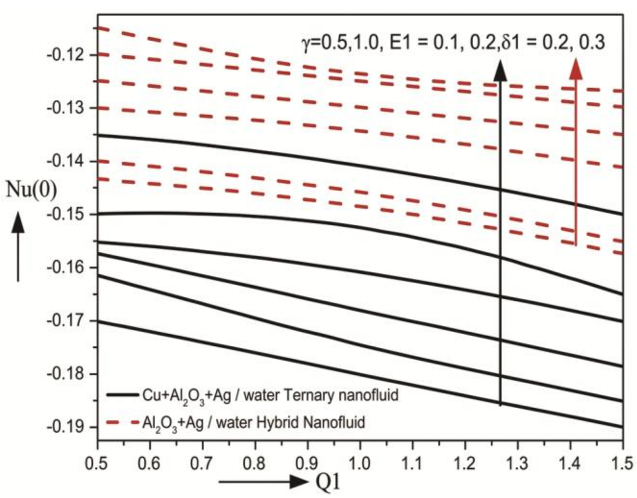

Fig. 16 — Variation of Nusselt number (Nu) at η=0 with Q1, γ, E1, and δ

rises with increasing chemical reaction parameter (γ), activation energy (E1), and temperature difference ratio (δ) in both nanofluid kinds.

Nomenclature

a, T_r	Constants	$\nu = \frac{\mu}{\rho}$	kinematic viscosity (m^2s^{-1})
ρ	fluid density (kgm^{-3})	μ	Dynamic viscosity (pas^{-1})
C_p	specific heat at constant pressure ($Jkg^{-1}K^{-1}$)	A11	The space-dependent internal heat source/sink factor
C_f	Skin friction coefficient	γ	Chemical reaction parameter
C	fluid concentration (Kg/m^3)	k^*	coefficient of mean absorption
A33	Slip parameter	θ_r	Viscosity parameter
k	Thermal conductivity ($Wm^{-1}K^{-1}$)	B11	the temperature-dependent heat source/sink factor
Rd	Thermal radiation factor	Q1	radiation absorption parameter
M	Magnetic parameter	σ^*	Stefan-Boltzmann constant
N	Buoyancy ratio	D_B	Brownian diffusion coefficient

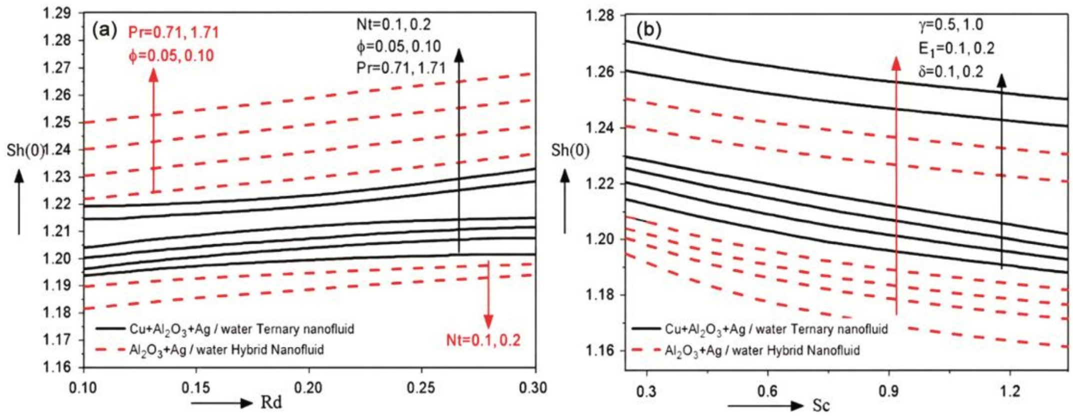

Fig. 17 — Variation of Sherwood number (Sh) at η=0 with (a) Rd, Nt, ϕ, Pr; and (b) Sc, γ, E1, and δ

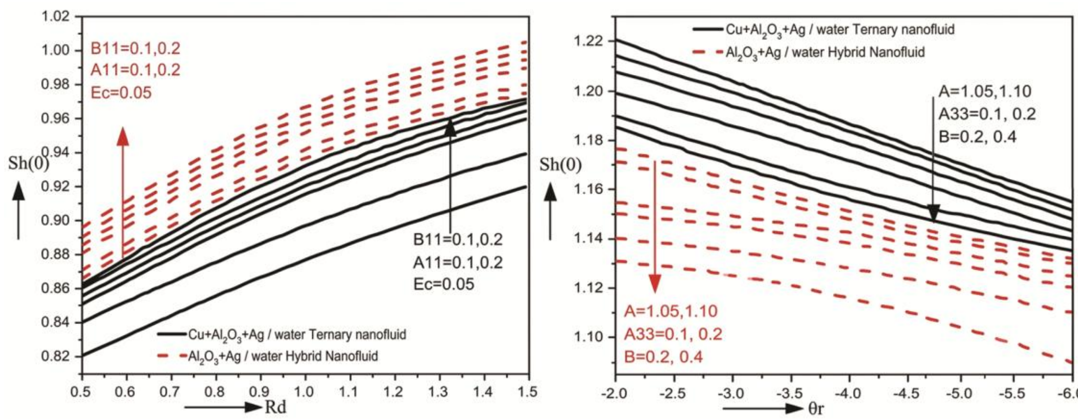

Fig. 18 — Variation of Sherwood number (Sh) at η=0 with (a) Rd, B11, A11, and Ec; and (b) θr, A, A33, and B

D_T	Thermophoretic diffusion coefficient	C_∞	Ambient concentration (Kg/m^3)
T_∞	Ambient temperature(K)	A	non-linear thermal radiation
q_r	Radiative heat flux vector (W/m²)	Nb	Brownian motion parameter
Nt	Thermophoresis parameter	Le	Lewis number
β	Velocity slip parameter	Ec	Eckert number
Pr	Prandtl number	Re_x	Reynolds number
E1	Activation energy	δ	Temperature difference parameter
$\vec{B}$	magnetic induction vector	h1	convective heat transfer constant
B_0	strength of applied magnetic field	m	Hall parameter
n	Index number	(u, v, w)	the velocity components along the (x, y, z)
fs	Forchheimer parameter	K	Porosity parameter
R	Rotation parameter	Ω	Angular velocity of the rotating system (rad/s)

Conclusion

- The axial and secondary velocities decrease with increasing magnetic field (M), activation energy (E_1), nanoparticle volume fraction (ϕ), and resistive parameters, while increasing with Hall parameter (m), Eckert number (Ec), Brownian motion (Nb), thermophoresis (Nt), and chemical reaction (γ).
- The opposite effect of heat source characteristics (A_{11}, B_{11}) and Prandtl number (Pr) on velocity components in nanofluids is observed: axial velocity increases while secondary velocity decreases, indicating asymmetric momentum transmission.
- Thermophysical factors such as thermal radiation, viscous dissipation, and nanoparticle activity enhance temperature, while convective cooling, buoyancy, and non-linear radiation lower it.
- Nanoparticle concentration increases with heating (A_{11}, B_{11}, Ec) and decreases with increased viscosity (θ_r), thermodiffusion (Nt), and radiation

absorption (Q_1), indicating complicated mass transport controlled by energy and resistance mechanisms.
- Stress components (τ_x, τ_z) rise with rotation (R), Hall current (m), slip (A_{33}), and heat sources but reverse with viscosity and buoyancy, indicating layered shear effects.
- Nusselt number (Nu) increases with activation energy (E_1) and chemical reaction (γ), showing positive feedback between reaction kinetics and heat transport, unlike usual resistive metrics like viscosity, radiation, and absorption.

Future scope
- This study can be used on non-Newtonian fluids to examine complex behaviors like shear-thinning, shear-thickening, and viscoelastic effects in nanofluid systems.
- Unsteady flow conditions are crucial for understanding time-dependent and startup behaviors in thermal and fluid systems.
- Optimization and machine learning methods can enhance heat and mass transmission in nanofluid technologies by identifying optimal parameter combinations.
- The model is adaptable to three-dimensional geometries, curved surfaces, and rotating frames, making it helpful for industrial systems like turbines, heat exchangers, and biomedical equipment.

Limitations and practical considerations

Although the present analysis offers a comprehensive numerical portrait of a rotating Cu–Al_2O_3–Ag/water ternary nanofluid over a stretching sheet, several caveats merit explicit acknowledgement.
- The formulation presupposes a steady, laminar and incompressible regime; turbulent fluctuations, unsteady transients and compressibility effects - features inherent to many high-Reynolds-number industrial flows are not captured.
- The single-phase model enforces local thermal equilibrium between base fluid and dispersed nanoparticles, an idealisation that may break down in highly dynamic or strongly non-isothermal environments.
- The conclusions rest exclusively on numerical integration of the boundary-layer equations and have not yet been corroborated by laboratory measurements; departures arising from impurities, manufacturing tolerances and other non-ideal conditions are therefore not quantified.
- The stretching-sheet geometry, while representative of a wide class of polymer-processing and metal-forming operations, does not encompass curved, irregular or three-dimensionally complex surfaces encountered in turbomachinery and biomedical microfluidics.
- The investigation is restricted to one specific ternary combination (Cu + Al_2O_3 + Ag in water); alternative nanoparticle triplets (e.g. CuO–TiO_2–SiO_2, graphene–Fe_3O_4–Ag) and non-aqueous base fluids (ethylene glycol, transformer oil) may exhibit qualitatively different transport behaviour and warrant separate study.
- The long-term colloidal stability of ternary suspensions, notably the propensity for nanoparticle agglomeration, sedimentation and surface fouling under prolonged operation is not addressed in the present model, yet remains decisive for industrial deployment.
- The cost-effectiveness, scalability and environmental footprint of the constituent nanoparticles deserve critical evaluation: silver and copper nanoparticles, in particular, raise documented concerns regarding aquatic toxicity, bioaccumulation and disposal that must be weighed against their thermal benefits.
- Although a parallel comparison with the binary Al_2O_3–Ag/water hybrid nanofluid is presented throughout, the present work does not contrast the ternary system with mononanofluids or with competing advanced cooling technologies such as microchannel heat sinks, phase-change materials or pulsating heat pipes; such benchmarking would strengthen the engineering case for ternary suspensions.
- Finally, external disturbances commonly encountered in service environments, mechanical vibrations, fluctuating magnetic fields and time-varying heat sources are absent from the present formulation.

These limitations collectively delineate a clear roadmap for future experimental validation, multi-phase modelling, geometric generalisation and techno-economic assessment.

Acknowledgement

This research was not funded by any grant.

Conflict of interest

All authors declare no conflict of interests.

References

1 Crane LJ, Boundary layer flow due to a stretching cylinder. *Z Angew Math Phys*, 26 (1975) 619.
2 Wang CY, Fluid flow due to a stretching cylinder. *Phys Fluids*, 31 (1988) 466.
3 Ahmad S, Hayat T, Alsaedi A, Ullah H & Shah F, Computational modeling and analysis for the effect of magnetic field on rotating stretched disk flow with heat transfer. *Propuls Power Res*, 10 (2021) 48.
4 Ishak A, Nazar R & Pop I, Magnetohydrodynamic (MHD) flow and heat transfer due to a stretching cylinder. *Energy Convers Manage*, 49 (2008) 3265.
5 Choi SUS, Enhancing thermal conductivity of fluids with nanoparticles. *ASME Fed*, 231 (1995) 99.
6 Buongiorno J, Convective transport in nanofluids. *J Heat Transfer*, 128 (2006) 240.
7 Hayat T & Nadeem S, Heat transfer enhancement with Ag–CuO/water hybrid nanofluid. *Results Phys*, 7 (2017) 231.
8 Waqas H, Ali Khan S & Muhammad T, Thermal analysis of magnetized flow of AA7072–AA7075/blood-based hybrid nanofluids in a rotating channel. *Alex Eng J*, 61 (2022) 3059.
9 Devi SSU & Devi SPA, Numerical investigation of three-dimensional hybrid Cu–Al_2O_3/water nanofluid flow over a stretching sheet with Lorentz force under Newtonian heating. *Can J Phys*, 94 (2016) 490.
10 Acharya N, Maity S & Kundu PK, Influence of inclined magnetic field on the flow of condensed nanomaterial over a slippery surface: the hybrid visualization. *Appl Nanosci*, 10 (2020) 633.
11 Usman M, Hamid M, Zubair T, Rizwan Ul Haq & Wang W, Cu–Al_2O_3/Water hybrid nanofluid through a permeable surface in the presence of nonlinear radiation and variable thermal conductivity via LSM. *Int J Heat Mass Transfer*, 126 (2018) 1347.
12 Aly EH & Pop I, MHD flow and heat transfer near stagnation point over a stretching/shrinking surface with partial slip and viscous dissipation: Hybrid nanofluid versus nanofluid. *Powder Technol*, 367 (2020) 192.
13 Khan MI, Khan SA, Hayat T, Khan MI & Alsaedi A, Arrhenius activation energy impact in binary chemically reactive flow of TiO_2–Cu/H_2O hybrid nanomaterial. *Int J Chem React Eng*, 17 (2019) 180183.
14 Mousavi S, Esmaeilzadeh F & Wang X, Effects of temperature and particle concentration on thermophysical and rheological behavior of CuO/MgO/TiO_2 ternary hybrid nanofluid. *J Therm Anal Calorim*, 137 (2019) 879.
15 Sahoo RR & Kumar V, Development of a new correlation to determine viscosity of ternary hybrid nanofluid. *Int Commun Heat Mass Transfer*, 111 (2020) 104451.
16 Chandrakala P & Srinivasa Rao V, Influence of dissipation and chemical reaction on heat and mass transfer in ternary nanofluids over a stretching sheet in porous media. *Int J Ambient Energy*, 46 (2025) 1.
17 Ullah I, Shafie S & Khan I, Effects of slip condition and Newtonian heating on MHD flow of Casson fluid over a nonlinearly stretching sheet in porous medium. *J King Saud Univ Sci*, 29 (2016) 1.
18 Hayat T, Imtiaz M, Alsaedi A & Kutbi M, MHD three-dimensional flow of nanofluid with velocity slip and nonlinear thermal radiation. *J Magn Magn Mater*, 396 (2015) 31.
19 Jusoh R, Nazar R & Pop I, Three-dimensional flow of nanofluid over a permeable stretching/shrinking surface with velocity slip: A revised model. *Phys Fluids*, 30 (2018) 033604.
20 Krishna MV, Ahamad NA & Chamkha AJ, Hall and ion slip impacts on unsteady MHD convective rotating flow of heat generating/absorbing second grade fluid. *Alex Eng J*, 60 (2021) 845.
21 Roy N & Pal D, Influence of activation energy and nonlinear thermal radiation with Ohmic dissipation on heat and mass transfer of Casson nanofluid over stretching sheet. *J Nanofluids*, 11 (2022) 819.
22 Yesodha P, Reddy PS & Chamkha AJ, Nanofluid flow with activation energy and heat generation/absorption effects over a stretching surface under convective boundary conditions. *Mater Today Proc*, 68 (2022) 112.
23 Sardar B, Ali SI, Muqaddas R & Ilyas K, Impact of activation energy on Carreau nanofluid flow over a nonlinear stretching surface. *J King Saud Univ Sci*, 36 (2024) 102711.
24 Khan MI, Hayat T, Khan MI & Alsaedi A, Activation energy impact in nonlinear radiative stagnation point flow of Cross nanofluid. *Int Commun Heat Mass Transfer*, 91 (2018) 216.
25 Tong ZW, Khan SU, Vaidya H, Rajashekhar, Sun TC, Khan MI, Prasad KV, Chinram R & Aly AA, Nonlinear thermal radiation and activation energy significances in slip flow of bioconvection of Oldroyd-B nanofluid with Cattaneo–Christov theory. *Case Stud Therm Eng*, 26 (2021) 1.
26 Hayat T, Imtiaz M, Alsaedi A & Kutbi M, MHD three-dimensional flow of nanofluid with velocity slip and nonlinear thermal radiation. *J Magn Magn Mater*, 396 (2015) 31.
27 Abo-Eldahab EM & Salem AM, Hall effects on MHD free convection flow of non-Newtonian power-law fluid at a stretching surface. *Int Commun Heat Mass Transfer*, 31 (2004) 343.
28 Shit GC & Haldar R, Combined effects of thermal radiation and Hall current on MHD free convective flow over a stretching sheet with variable viscosity. *J Appl Fluid Mech*, 5 (2012) 113.
29 Chamkha AJ, Mansour MA & Aly AM, Unsteady MHD free convective heat and mass transfer from a vertical porous plate with Hall current, thermal radiation and chemical reaction. *Int J Numer Methods Fluids*, 65 (2011) 432.
30 Animasaun I, Effects of thermophoresis, variable viscosity and thermal conductivity on MHD Casson fluid flow with suction and chemical reaction. *J Niger Math Soc*, 34 (2015) 11.
31 Abd El-Aziz M, Temperature dependent viscosity and thermal conductivity effects on combined heat and mass transfer in MHD flow over stretching surface. *Meccanica*, 42 (2007) 375.
32 Lund LA, Omar Z, Dero S, Baleanu D & Khan I, Rotating 3D flow of hybrid nanofluid on exponentially shrinking sheet: Symmetrical solution and duality. *Symmetry*, 12 (2020) 1637.
33 Shahzadi M, Kousar U, Zubair M & Malik MY, Thermal flow of Al_2O_3–Cu–Ag/Water nanofluid over a stretching surface: activation energy and temperature-dependent viscosity effects. *Case Stud Therm Eng*, 58 (2025) 105523.